Radiomics-Led Monitoring of Non-Small Cell Lung Cancer Patients During Radiotherapy

Roushanak Rahmat[1,2,4,5,6], David Harris-Birtill[2], David Finn[3], Yang Feng[4], Dean Montgomery[4], William H Nailon[4,5], and Stephen McLaughlin[6]

[1] Computational Imaging Group, The Institute of Cancer Research, London, UK
[2] School of Computer Science, University of St Andrews, UK
[3] Department of Radiation Oncology, Western General Hospital, Edinburgh, UK
[4] Department of Oncology Physics, Western General Hospital, Edinburgh, UK
[5] School of Engineering, the University of Edinburgh, Edinburgh, UK
[6] School of Engineering and Physical Sciences, Heriot-Watt University, Edinburgh, UK

Abstract. Co-locating the gross tumour volume (GTV) on cone-beam computed tomography (CBCT) of non small cell lung cancer (NSCLC) patients receiving radiotherapy (RT) is difficult because of the lack of image contrast between the tumour and surrounding tissue. This paper presents a new image analysis approach, based on second-order statistics acquired from grey level co-occurrence matrices (GLCM) combined with level sets, for assisting clinicians in identifying the GTV on CBCT images. To demonstrate the potential of the approach planning CT images from 50 NSCLC patients were rigidly registered with CBCT images from fractions 1 and 10. Image texture analysis was combined with two level set methodologies and used to automatically identify the GTV on the registered CBCT images. The Dice correlation coefficients ($\mu \pm \sigma$) calculated between the clinician-defined and image analysis defined GTV on the planning CT and the CBCT for three different parameterisations of the model were: 0.69 ± 0.19, 0.63 ± 0.17, 0.86 ± 0.13 on fraction 1 CBCT images and 0.70 ± 0.17, 0.62 ± 0.15, 0.86 ± 0.12 on fraction 10 CBCT images. This preliminary data suggests that the image analysis approach presented may have potential for clinicians in identifying the GTV in low contrast CBCT images of NSCLC patients. Additional validation and further work, particularly in overcoming the lack of gold standard reference images, are required to progress this approach.

Keywords: Image Segmentation · Level Set · Radiomics · Radiotherapy · Lung Cancer.

1 Introduction

In 2014, there were 46,400 new cases of lung cancer in the United Kingdom (UK) and 35,900 deaths were directly attributable to this disease [1]. Treatment options include radiotherapy (RT) in which a high radiation dose is delivered to cancerous tissue whilst the radiation dose to healthy tissue is minimised [2]. In radiation treatment planning, manual segmentation of the region of interest is typically based on the visual evaluation of CT images. The correctness of the delineated volume is depending on the capability to visualise the tumour and identify its surrounding regions.

At time-of-treatment CBCT images are used for patient alignment by identifying the position of landmarks such as bone [3]. However, establishing the location of the GTV on CBCT images is

extremely challenging because of the poor soft tissue contrast. Furthermore, it is currently not feasible to estimate changes in the GTV on CBCT that are because of the disease progression or in response to radiation treatment. These problems limit the use of CBCT in NSCLC for adapting, or personalising treatment, where the planned dose to healthy tissue and the planned dose to the tumour are preserved.

The utilization of image semi-automatic or fully-automatic segmentation techniques can assist in improving the accuracy and decreasing the length of time conjugated determining radiation target volume and organs at risk (OAR) of damage from radiation. However, segmenting tumours, and OARs, on CT and CBCT images is challenging and the purpose of this work was to develop a radiomics-based approach for analysis of CBCT images for (1) automatically identifying the GTV on follow-up images (CBCT) and (2) detecting significant changes in shape and size indicative of progression of disease or radiotherapy response. In relation to this, a bespoke image segmentation framework was developed that combined image texture analysis with level set analysis, which is shown in Figure 1. The framework has the potential to lead to improvements in radiation targeting when the morphology of the tumour has changed, which could be practice changing. At present changes in tumour morphology are analysed after specific fractions of RT throughout the course of treatment [4]. Here this was done at the 10th day of treatment, that is the fraction 10 (#10), when a volumetric CBCT image set was acquired and algorithm applied. The central hypothesis proposed here was that the texture of a cancerous region changes in response to radiation, which can be detected by texture/radiomics analysis. To ensure that the radiomics analysis was performed only on the tumour volume an exquisite level set model introduced in [5], that merges two or more different techniques of level set in parallel, was used.

In this paper, an overview of the proposed technique is presented in section 2 and the framework for monitoring NSCLC cancer. Further on, this section provides a focused literature review covering the texture analysis and level set models used. Section 3 provides details of the dataset, including contouring information, and the registration procedure used. Finally, section 4 presents the results obtained following application of the framework to a large cohort of patients and ground truth data, which was available for one of the patients.

2   Overview of the combined level set model with texture analysis

The proposed framework in monitoring lung cancer during RT is shown in Figure 1. The process begins with the registration of the CBCT acquired at fraction 1, (#1) to the planning CT image on which the GTV is defined. This provides a set of parameters for starting the combined level set with texture analysis for segmentation of CBCT #1. A Dice similarity coefficient, typically greater than 90%, is then used to assess the similarity between the GTV on the planning CT and the CBCT. Such a high value is used because the CBCT #1 images are acquired before radiation therapy started and therefore before any change in shape as a result of radiation. A similar approach was used for the segmentation of the GTV on CBCT #10 and on the planning-CT images, however, because this CBCT scan takes place at the 10th day of treatment. Therefore, less similarity is expected between CBCT images and the planning CT. Consequently, the Dice score value was reduced to 70%. With these settings if the likeliness and correspondence is far more than the selected threshold, therefore radiotherapy should be continued but if far less, it is

an indication that there has been a significant change in the GTV and repositioning, or further investigation, is required.
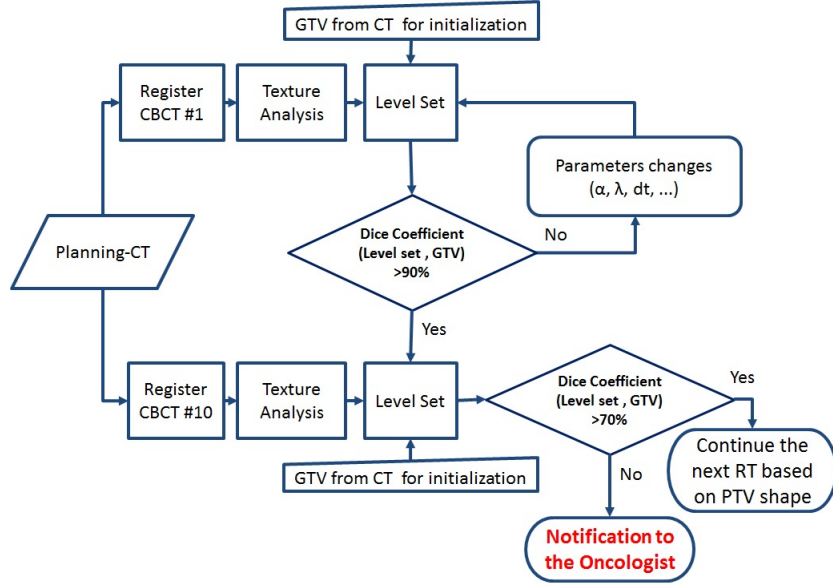

Fig. 1: The proposed framework for tracking the effect of treatment for the lung cancer during radiation therapy using a combined level set technique with texture analysis, which can be used for detecting large deviations in the GTV on CBCT images.

There are many different level set techniques each with propagation characteristics that may be suited to particular applications and there are several review articles covering the use of these techniques in different imaging applications. These include region based image segmentation in [6], medical imaging in [7] and [8], optimal design and inverse problems in [9], piecewise constant applications in [10], deformable models in [11] and [12]. There are also comprehensive reviews covering more general level set applications in [13], [14], [15] and [16]. What is common in all of these articles is that each path is powerful to a particular application but not for every types of images, which is a problem in complex medical images.

In general, a level set technique defines an evolving boundary by setting up a zero level set for a higher dimension for ϕ function. The z axis which represent the height of the level set represents the minimum distance at each point in the Cartesian coordinate from the contour C. To begin this propagating function we need to initialize it. An initial value for initialization process is needed which can be selected semi-automatically or fully-automatically. Also, depending on the two or multiple number of different regions or phases required in the image segmentation task, the initial values are needed. The two-phase level set models patrician the image into two different regions without overlapping pixels. While multi-phase level set (three or four-phase) patrician the image into multiple regions (three or four phases respectively) by utilizing two unrelated level set models together. Re-initialization is recurred during evolution to withhold

the happening of sharp corners. This can be done by computing new values of ϕ based on the defined speed function.

Chan and Vese extended the Osher-Sethian model in the 1990s by using the energy minimization term which provides automatic segmentation of interior regions [17]. This is accomplished by using a technique introduced by Mumford-Shah [18] based on the piecewise constant and piecewise smooth optimal approximations. In [17], further modifications resulted in a level set method in two-phase for two-region segmentation which does not have the edges like the primary representation of level set. The Chan-Vese model in two-phase measures the mean intensity values for each one of the two phases which are the inside and outside of the segmentation region in the image. In 2000, Chan and Vese extended the two-phase model for the applications of vector-valued images, that performed steadily on the noisy images [19]. The vector-valued based model is commonly used in coloured or texture imaging and video image processing for tracking objects and texture images. They even extended their model further in 2002 to a multi-phase level set model that calculates the log numbers of the level set functions to segment n regions by using piecewise constant [20]. The initialization of each level set Multi-Phase Chan-Vese function is done independently and separately but the same function for level set is used for all initialisations.

The Li level set model is another popular and robust model, which has developed different forms based on gradient flow for overcoming the intensity inhomogeneity as an edge based method in level set [21,22,23]. Li's model applies the energy minimization procedure used in snake model, by minimizing the fitting energy of the segmentation.

2.1   Parallel Vector-Valued Level Set Model

We recently proposed a novel level set model in [5] which had the least amount of dependency to the parameter setting. This model is most useful for the type of image where there is a lack the ground truth information. This model takes advantage of the presence of existing models by combining them in vector-valued imaging or multi-phase. Also, level set in segmentation of the tumour infiltration boundary showed robust performance in construction of radiotherapy target volumes [24].

Here, texture analysis was implemented as a pre-segmentation technique before applying the main segmentation model based on the level set. It has been previously reported that the healthy tissues' texture is distinct from the texture of cancerous tissues [25] and the texture may also change within these regions during the course of radiotherapy. There are many different ways of calculating texture features such as [26], [27], [28] and [29]. In this paper, second-order statistics were applied using the GLCM approach. In 1979, first introduced by Haralick [26], this statistical measurements are used to compute the 2nd-order statistical features for texture and commonly 14 features are calculated. A modified GLCM approach proposed by Randen [30], which uses histogram-equalising, was also used in this work.

3   Tests conducted on NSCLC cohort

Images from 50 patients suffered from lung cancer and been treated with RT at the Edinburgh Cancer Centre, Edinburgh, UK between 2010 and 2011 were used in this study. Planning CT

images were available for all patients and CBCT images acquired at #1 and #10. All CT images were acquired with 512×512 pixels with the pixel size of 0.977mm×0.977mm. All CBCT images were acquired with 384×384 pixels with the pixel size of 1.172mm×1.172mm. The quantity of slices for the CT and CBCT images which contain the tumour volume was different in the dataset for different patients. A radiation oncologist evaluated all images and the outlined the GTV, clinical tumour volume (CTV), planning tumour volume (PTV) and organs at risk (OAR).

Special attention was given to CBCT #10, which is the point where the patient has received approximately 30% of their treatment and where an indication of response to treatment would be extremely valuable. In Figure 2, the planning-CT and its corresponding CBCT #1 and #10 for one of the patients in the dataset are shown. In Figure 2 a red contour illustrates the GTV on the CT and CBCT images. This figure highlights the difference in tumour volume between these images.
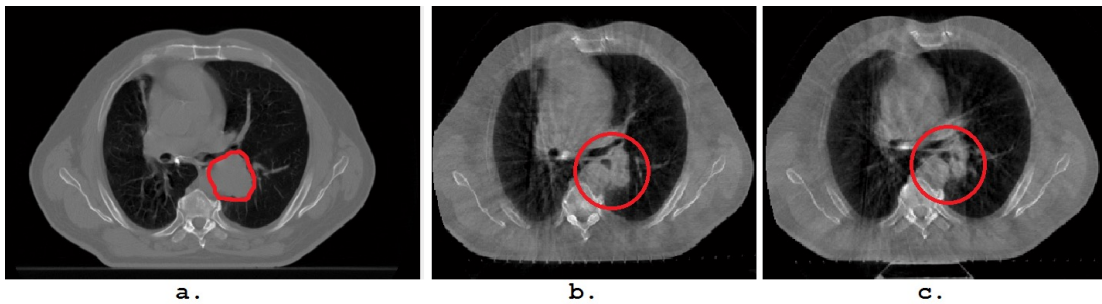

Fig. 2: Mapping of the GTV over the course of treatment: a. single slice of the planning-CT along the red contour for GTV boundry, b. CBCT #1 acquired before any radiotherapy is given(thirteen days after the planning CT) and c. the CBCT #10, 26 days after the initial planning CT.

3.1   Registration CBCT to CT

Registration is an essential and important step in medical image processing. This assists the clinicians to evaluate different images acquired at different time intervals or from different modalities. Also, it is very difficult to extract the translation between different images to align them properly. In RT, radiographers acquire the CBCT images and file the change in the position of a patient with its relevant planning-CT. They need to register CBCT images to the planning-CT images before radiating the patient. Having access to this transformation matrix for the registration is essential in mapping the GTV delineated by the clinicians on the planning-CT to CBCT images.

The image registration process of CBCT with the CT by a radiographer results in a transformation matrix, which was considered as the clinical gold standard transform. This transformation matrix consists of 3 different transformations. When CBCT are translated to CT coordinate, first a transformation is needed to bring them to the centre of the CBCT. After this, they can be translated based on the image by considering patient orientation and patient position.

Then, the file stored from the radiology translation attached to the CBCT can be extracted. This provides the distance between CBCT and CT in different rectangular coordinate space to translate the CBCT into the origin of CT's space. The final affine transform in this translation is using the meta data of the CT images which recorded the position of the patient during scanning in regards to their origin of CT space. The meta data for the CBCT data also have the information needed for this affine transform in terms of rotation and translation of the patient position compared to their planning-CT scan.

As shown in Figure 3, three affine transforms of T_1, T_2 and T_3 are performed. These 4×4 matrices are the main components needed to map between the CBCT and CT images. Both of T_1 and T_2 matrices are computed based on Equation 1 using meta data embedded in the DICOM images from the reference and target images respectively. The final metric of T_3 is extracted from the reference coordinate system (RCS) that are provided by the meta data embedded in the CBCT's DICOM images.
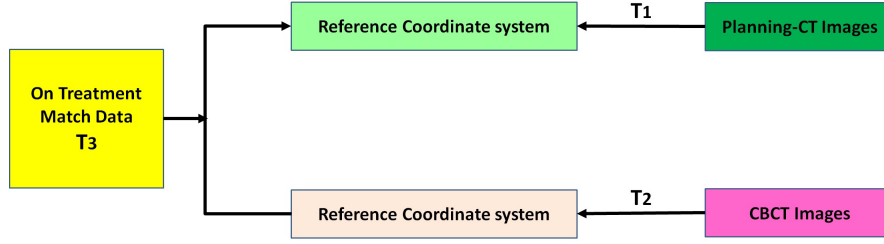

Fig. 3: The process of CBCT image registration to planning-CT images is performed using the RT information determined by radiographers at time-of-treatment. The translation between the planning-CT which is the reference image to the CBCT which are the target image as well as their RCS which are embedded in the image meta information are all used to find the transformation matrix of image registration. In this illustration T_1 refers to the affine transform of planning-CT to the RCS, T_2 shows the CBCT to RCS transformation and T_3 provides the final transformation from the RCS of the CBCT images to the RCS of the CT image.

$$T_1 = \begin{bmatrix} X_x \Delta i & Y_x \Delta j & 0 & S_x \\ X_y \Delta i & Y_y \Delta j & 0 & S_y \\ X_z \Delta i & Y_z \Delta j & 0 & S_z \\ 0 & 0 & 0 & 1 \end{bmatrix} \tag{1}$$

S_x, S_y and S_z are the elements of this matrix which are obtained from the DICOM tag for the Image Position Patient, that provides the distance from the RCS origin mm. Also, X_x, X_y and X_x show the first three elements in the DICOM Image Orientation Patient. Y_x, Y_y and Y_z are the final three elements of the DICOM Image Orientation Patient. The values of Δi and Δj refer to the pixel size in each image, which are also embedded in the DICOM meta information. At last, by measuring the T_3 based on the RT registration file recorded by the radiographers, we can calculate the final transformation needed for this registration T. Equation 2 shows this rigid registration to calculate the T which is the gold standard in this process.

$$T = T_1^{-1} T_3 T_2 \tag{2}$$

From the initial planning CT scan to radiotherapy at each fraction patients are positioned in exactly the same way. Throughout treatment patients are aligned to reference tattoos made

on the skin surface, which make lateral adjustments straightforward through couch shifts. No rotational adjustment was made for the cohort of patients used here.

4   Results and Discussion

Radiomics provides a nice range of 1st order, 2nd order statistical features to exploit the relationships between image voxels,size and shape based–features, image intensity histogram feature and fractal features [31,32,33]. We have selected the 2nd order Haralick features in 3D lung volumes to calculate feature maps in voxel-based [34,35].
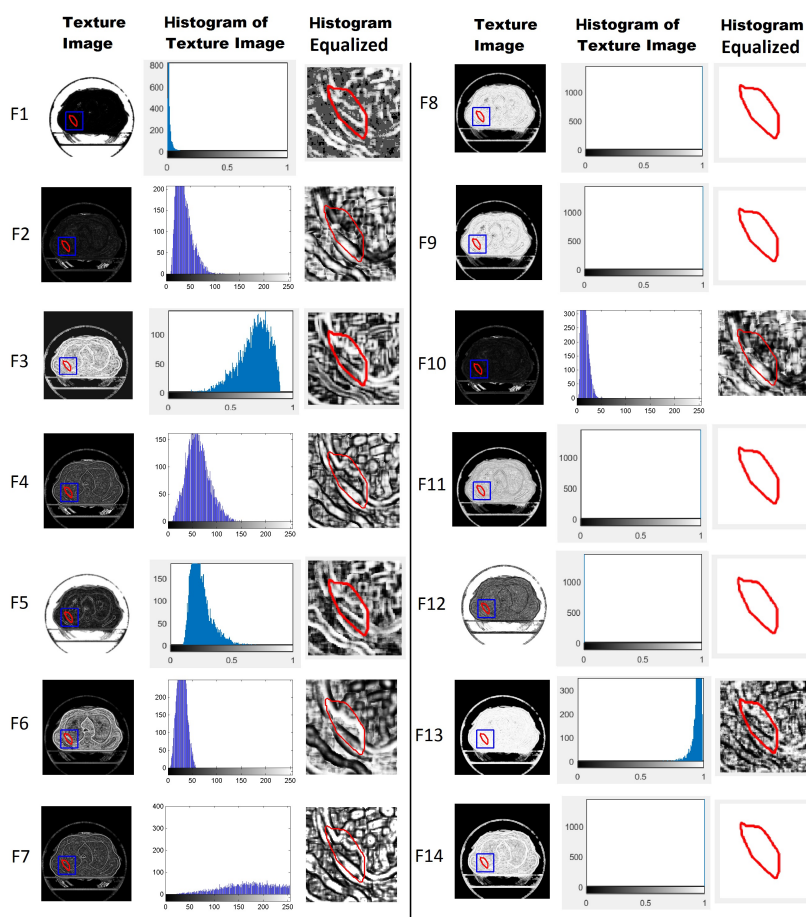

Fig. 4: Haralick texture results for one of the dataset patient's CBCT #1, F1: angular second moment, F2: contrast, F3: correlation, F4: variance, F5: inverse difference moment, F6: sum average, F7: sum variance, F8: sum Entropy, F9: entropy, F10: difference variance, F11: difference entropy, F12: information measures of correlation, F13: information measures of correlation and F14: maximal correlation coefficient.

8   R. Rahmat et al.

To identify the best texture features the GLCM approach was applied in four symmetric directions in a 5×5 region. Feature values were equalised to enable comparison and CBCT images were converted to unit8 format. Of the fourteen texture features, several were found to be highly correlated, which would result in a low-qulaity input for level set convergence. The best texture feature that could be combined with Chan-Vese method was found to be the sum variance, which had the best distributed intensity levels among all texture images. Figure 4 illustrates the fourteen Haralick texture images the GTV of CTV shown in red. It also shows, the histogram and the equalised histogram image of CBCT #1 for each texture image. From this figure, we can see that F7 which is the sum variance is the single texture image with an smooth histogram. F7 texture image also shows the tumour boundaries are more visible compared to other features.

Figure 4 also shows that many of the features are not suitable for this experiment. For instance, F14 and F12 feature may interrupt the effect of other features when they are merged together. This can be explained as these texture features have a narrow span of intensity values as shown in F1, F3, F5, F8, F9, F11, F12, F13 and F14. On the other hand F7 can provide adequate intensity variation and saves more of the dynamic range of the change in intensity as shown in Figure 4.
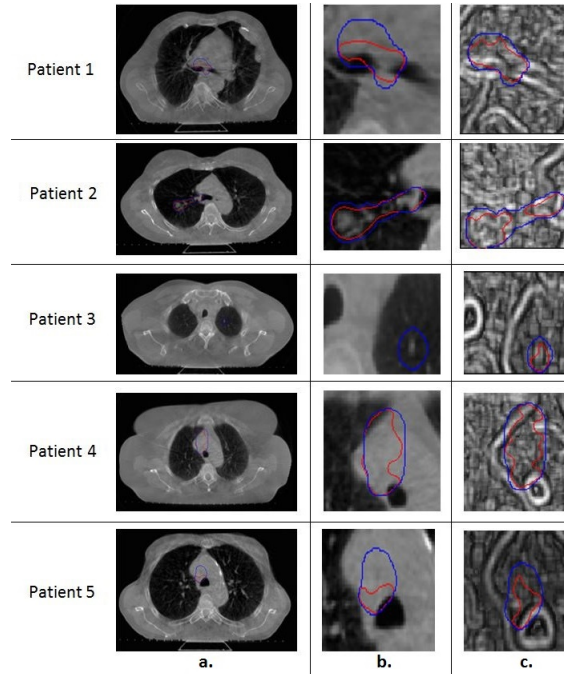

Fig. 5: A comparison of applying the proposed level set model on the registered CBCT images as well as applying them on their textured images for 5 different patients, a. CBCT image in full size with the GTV and level set segmentation contour, b. CBCT image cropped to illustrate better the level set segmentation performance and c. The texture (sum variance) image cropped showing the segmentation contour obtained from applying level set on this image (red contour demonstrates level set and blue contour shows GTV).

Figure 5 illustrates five different patients having CBCT images and their segmentations obtained by Chan-Vese level set in absence and presence of applying sum variance texture on the image. In column b, we can see the segmentation outcome of level set on the CBCT images compared to column c when level set was applied on the texture image (sum variance). Among all of the 14 Haralick texture features used on this data, the sum variance regularly provide the finest results. Figure 5 shows that there is a small tumour for Patient 3 which was not detected by the clinicians while the proposed method of level set combined with sum variance detected it. Texture images are more probable to provide a premier starting point for the level set as the target region (cancerous cells and tissues around them) is changing during RT.

4.1   Assessing the clinical performance without a ground truth

One of the challenges of this work was the absence of ground truth on the true location of the GTV on the CBCT images. In other words, how do we know which method for automatically identifying the GTV is the best? To investigate this further and to investigate the impact of different parameterisations of the model on the final GTV contour different combinations were tested and the results presented to an experienced a radiation oncologist. The different combinations tested were:

1. Sum variance + Parallel level set (Model 1)
2. Sum variance + Chan–Vese level set (Model 2)
3. Sum variance + Li level set (Model 3)

The performance of the proposed combined models, is illustrated in Figure 6, depends on three factors: initialisation of the GTV, the calculated sum variance image and the parameters selection. The parameter tuning is an important aspect of level set models, accordingly selecting these parameters can affect the convergence of level set.
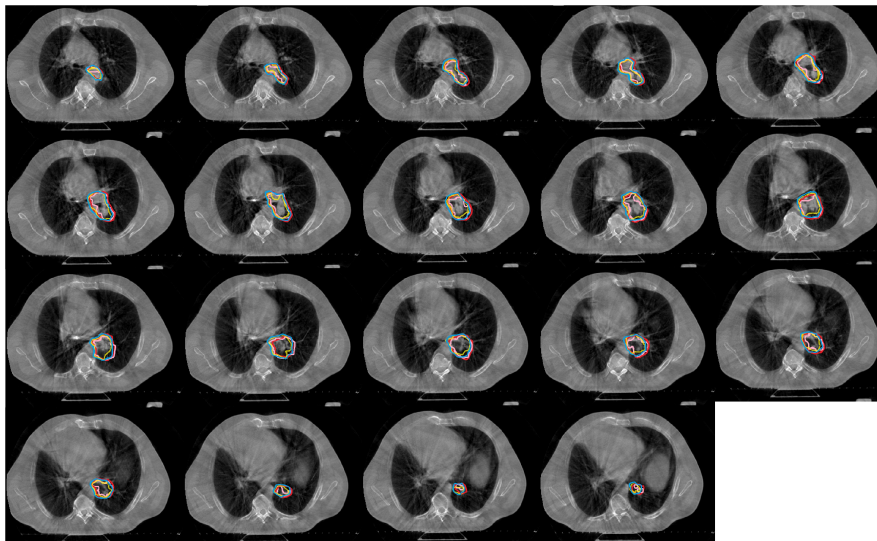

Fig. 6: Three best selected segmentations by the oncologist. Blue contour is GTV, pink refers to Model 1, red is Model 2 and yellow is Model 3.

Figure 7 shows the observation obtained from comparing the calculated Dice score among segmentation models and their planning-CT GTV for the whole dataset. The results for all of the fifty patients were provided to the oncologist on CBCT #10. From this comparison we can conclude that Model 2 could obtain the highest Dice score for that reveals the inability of it to depart from its initial point. Model 3 performs the best implementation of the segmentation taks on these images with more than 50% likeliness to the GTV on planning-CT.
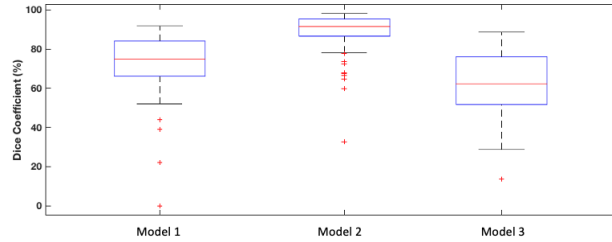

Fig. 7: The stability of our proposed level set models on CBCT #10 by evaluating the Dice score for the whole dataset (consisting of 10 patients) versus their GTV. All models were selected by the clinical oncologist. Model 2 is providing more satisfactory results than Model 3 and Model 1.

The position of the tumour in the lungs and its volume effect the outcome of the proposed combined model. Smaller tumours and more superior tumours in the lungs can be less influenced by patient breathing. Consequently the images are less affected or deformed in the breathing phases. The oncologist noted that any of our combined proposed model of level set and texture can be incorrect when the Dice score is small because the GTV could suffer precision. To evaluate this further the approach was tested in non-medical images.

4.2   Accessing performance on non-medical data with a ground truth

The proficiency of our proposed models was evaluated on non-medical images for the purpose of establishing accuracy and overall performance. The non-medical images were selected from the literature on level set papers which have ground truth data. The results are shown in Figure 8 as Cha-Vese, Li and Parallel (combined Li and Chan-Vese) level set methods.
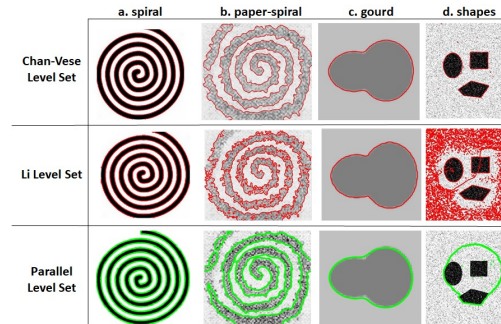

Fig. 8: Images of non-medical shapes: a. spiral, b. paper-spiral, c. gourd and d. shapes, used for the segmentation with different level set methods: Chan-Vese [17], Li [21] and parallel level set [5].
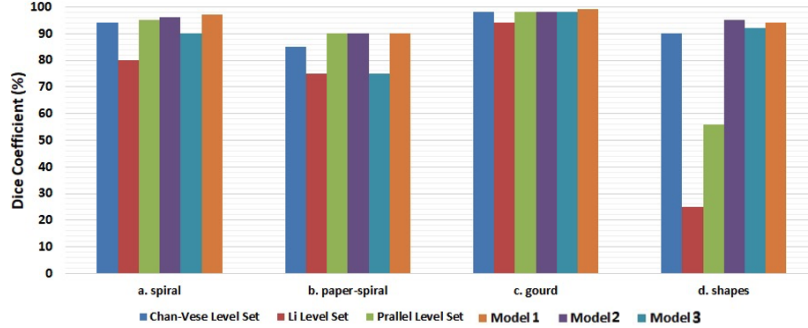
Fig. 9: Testing proposed texture+level set models (Model 1, Model 2 and Model 3) compared to the level set models without combining them with texture (Chan-Vese [17], Li [21] and parallel level set [5]), on four non-medical images which they all possess a ground truth: a. gourd, b. spiral, c. shapes and d. gradient-ball.

The presence of ground truth on the non-medical dataset provides a better evaluation on a more comprehensive and quantitative demonstration. The results in Figure 9 show the ability of the models (Model 1, Model 2 and Model 3) in segmentation and the improvement of the level set methods when combined with texture feature.

5   Conclusion

Assessing lung cancer patients during radiotherapy is very challenging because of the lack of contrast on CBCT images. With further validation the proposed approach for automatically evaluating non-small cell lung tumours using CBCT images has the potential to help oncologists for improving their assessment for the shape and size of tumours during a course of radiotherapy. However, there are multiple factors that must be considered when combining texture and a level set model. One of the most important factors is the importance of selecting the proper model that can functionally be combined and provide acceptable results on CBCT images of the lungs. The other important matter is related to the initialisation of the proposed models, where the level set performance is very much related to it. The final and most critical problem was selecting the parameters for the level set models that can impact its performance.

6   Acknowledgements

References

1. 2016 (accessed July 3, 2016). `https://www.cancerresearchuk.org/health-professional/cancer-statistics/statistics-by-cancer-type/lung-cancer`.

2. Inga S Grills, Di Yan, Alvaro A Martinez, Frank A Vicini, John W Wong, and Larry L Kestin. Potential for reduced toxicity and dose escalation in the treatment of inoperable non–small-cell lung cancer: A comparison of intensity-modulated radiation therapy (imrt), 3d conformal radiation, and elective nodal irradiation. *International Journal of Radiation Oncology* Biology* Physics*, 57(3):875–890, 2003.

3. Qiang Wen, Jian Zhu, Xue Meng, Changsheng Ma, Tong Bai, Xindong Sun, and Jinming Yu. The value of cbct-based tumor density and volume variations in prediction of early response to chemoradiation therapy in advanced nsclc. *Scientific reports*, 7(1):1–10, 2017.

4. V Grégoire and TR Mackie. State of the art on dose prescription, reporting and recording in intensity-modulated radiation therapy (icru report no. 83). *Cancer/Radiothérapie*, 15(6-7):555–559, 2011.

5. Roushanak Rahmat, William Henry Nailon, Allan Price, David Harris-Birtill, and Stephen McLaughlin. New level set model in follow up radiotherapy image analysis. In *Annual Conference on Medical Image Understanding and Analysis*, pages 273–284. Springer, 2017.

6. Yuting Jiang, Meiqing Wang, and Haiping Xu. A survey for region-based level set image segmentation. In *2012 11th International Symposium on Distributed Computing and Applications to Business, Engineering & Science*, pages 413–416. IEEE, 2012.

7. Jasjit S Suri and Kecheng Liu. Level set regularizers for shape recovery in medical images. In *Proceedings 14th IEEE Symposium on Computer-Based Medical Systems. CBMS 2001*, pages 369–374. IEEE, 2001.

8. Elsa Angelini, Yinpeng Jin, and Andrew Laine. State of the art of level set methods in segmentation and registration of medical imaging modalities. In *Handbook of biomedical image analysis*, pages 47–101. Springer, 2005.

9. Martin Burger and Stanley J Osher. A survey on level set methods for inverse problems and optimal design. *European journal of applied mathematics*, 16(2):263, 2005.

10. Xue-Cheng Tai and Tony F Chan. A survey on multiple level set methods with applications for identifying piecewise constant functions. *Int. J. Numer. Anal. Model*, 1(1):25–47, 2004.

11. Johan Montagnat, Hervé Delingette, and Nicholas Ayache. A review of deformable surfaces: topology, geometry and deformation. *Image and vision computing*, 19(14):1023–1040, 2001.

12. Jasjit S Suri, Kecheng Liu, Sameer Singh, Swamy N Laxminarayan, Xiaolan Zeng, and Laura Reden. Shape recovery algorithms using level sets in 2-d/3-d medical imagery: a state-of-the-art review. *IEEE Transactions on information technology in biomedicine*, 6(1):8–28, 2002.

13. Roushanak Rahmat and David Harris-Birtill. Comparison of level set models in image segmentation. *IET Image Processing*, 12(12):2212–2221, 2018.

14. Daniel Cremers, Mikael Rousson, and Rachid Deriche. A review of statistical approaches to level set segmentation: integrating color, texture, motion and shape. *International journal of computer vision*, 72(2):195–215, 2007.

15. Zubin C Bhaidasna and Sheetal Mehta. A review on level set method for image segmentation. *International Journal of Computer Applications*, 63(11), 2013.

16. G Vineetha and Gopu Darshan. Level set method for image segmentation: a survey. *IOSR J. Comput. Eng*, 8(6):74–78, 2013.

17. Tony Chan and Luminita Vese. An active contour model without edges. In *International Conference on Scale-Space Theories in Computer Vision*, pages 141–151. Springer, 1999.

18. David Bryant Mumford and Jayant Shah. Optimal approximations by piecewise smooth functions and associated variational problems. *Communications on pure and applied mathematics*, 1989.

19. Tony F Chan, B Yezrielev Sandberg, and Luminita A Vese. Active contours without edges for vector-valued images. *Journal of Visual Communication and Image Representation*, 11(2):130–141, 2000.
20. Luminita A Vese and Tony F Chan. A multiphase level set framework for image segmentation using the mumford and shah model. *International journal of computer vision*, 50(3):271–293, 2002.
21. Chunming Li, Chiu-Yen Kao, John C Gore, and Zhaohua Ding. Minimization of region-scalable fitting energy for image segmentation. *IEEE transactions on image processing*, 17(10):1940–1949, 2008.
22. Chunming Li, Chiu-Yen Kao, John C Gore, and Zhaohua Ding. Implicit active contours driven by local binary fitting energy. In *2007 IEEE Conference on Computer Vision and Pattern Recognition*, pages 1–7. IEEE, 2007.
23. Chunming Li, Rui Huang, Zhaohua Ding, J Chris Gatenby, Dimitris N Metaxas, and John C Gore. A level set method for image segmentation in the presence of intensity inhomogeneities with application to mri. *IEEE transactions on image processing*, 20(7):2007–2016, 2011.
24. Roushanak Rahmat, Frederic Brochu, Chao Li, Rohitashwa Sinha, Stephen John Price, and Raj Jena. Semi-automated construction of patient individualised clinical target volumes for radiotherapy treatment of glioblastoma utilising diffusion tensor decomposition maps. *The British journal of radiology*, 93(1108):20190441, 2020.
25. Fanny Orlhac, Michael Soussan, Kader Chouahnia, Emmanuel Martinod, and Irène Buvat. 18f-fdg pet-derived textural indices reflect tissue-specific uptake pattern in non-small cell lung cancer. *PLoS One*, 10(12):e0145063, 2015.
26. Robert M Haralick. Statistical and structural approaches to texture. *Proceedings of the IEEE*, 67(5):786–804, 1979.
27. Constantino Carlos Reyes-Aldasoro and Abhir Bhalerao. The bhattacharyya space for feature selection and its application to texture segmentation. *Pattern Recognition*, 39(5):812–826, 2006.
28. Timo Ojala, Matti Pietikainen, and Topi Maenpaa. Multiresolution gray-scale and rotation invariant texture classification with local binary patterns. *IEEE Transactions on pattern analysis and machine intelligence*, 24(7):971–987, 2002.
29. Norberto Malpica, Juan E Ortuño, and Andrés Santos. A multichannel watershed-based algorithm for supervised texture segmentation. *Pattern Recognition Letters*, 24(9-10):1545–1554, 2003.
30. Trygve Randen and John Hakon Husoy. Filtering for texture classification: A comparative study. *IEEE Transactions on pattern analysis and machine intelligence*, 21(4):291–310, 1999.
31. Karel GM Moons, Douglas G Altman, Johannes B Reitsma, John PA Ioannidis, Petra Macaskill, Ewout W Steyerberg, Andrew J Vickers, David F Ransohoff, and Gary S Collins. Transparent reporting of a multivariable prediction model for individual prognosis or diagnosis (tripod): explanation and elaboration. *Annals of internal medicine*, 162(1):W1–W73, 2015.
32. Martin Vallières, Alex Zwanenburg, Bodgan Badic, Catherine Cheze Le Rest, Dimitris Visvikis, and Mathieu Hatt. Responsible radiomics research for faster clinical translation, 2018.
33. RN Mahon, M Ghita, GD Hugo, and E Weiss. Combat harmonization for radiomic features in independent phantom and lung cancer patient computed tomography datasets. *Physics in Medicine & Biology*, 65(1):015010, 2020.
34. Alex Zwanenburg, Martin Vallières, Mahmoud A Abdalah, Hugo JWL Aerts, Vincent Andrearczyk, Aditya Apte, Saeed Ashrafinia, Spyridon Bakas, Roelof J Beukinga, Ronald Boellaard, et al. The image biomarker standardization initiative: standardized quantitative radiomics for high-throughput image-based phenotyping. *Radiology*, 295(2):328–338, 2020.
35. Alberto Traverso, Leonard Wee, Andre Dekker, and Robert Gillies. Repeatability and reproducibility of radiomic features: a systematic review. *International Journal of Radiation Oncology* Biology* Physics*, 102(4):1143–1158, 2018.